Interfacial effects on the superconducting properties of $LaSi_2$(112) films on Si(111)

Lixia Liu,[1,2] Guangyao Miao,[1,2] Bing Liu,[1,2] Pengfei Nan,[1] Yade Wang,[1,2] Binghui Ge,[3] Xuetao Zhu,[1,2,4] Fang Yang,[1] Weihua Wang,[1,*] and Jiandong Guo[1,2,4,5,†]

[1]*Beijing National Laboratory for Condensed Matter Physics and Institute of Physics, Chinese Academy of Sciences, Beijing 100190, China*

[2]*School of Physical Sciences, University of Chinese Academy of Sciences, Beijing 100049, China*

[3]*Institutes of Physical Science and Information Technology, Anhui University, Hefei 230601, China*

[4]*Songshan Lake Materials Laboratory, Dongguan, Guangdong 523808, China*

[5]*Beijing Academy of Quantum Information Sciences, Beijing 100193, China*

(Received 8 April 2019; revised manuscript received 25 September 2019; published 30 October 2019)

Superconducting films are fascinating due to their tunability associated with the interfacial effects. Here we report the superconductivity of single-crystalline $LaSi_2$(112) films epitaxially grown on Si(111) substrates, which exhibit the superconducting transition temperature (T_c) of 3.2 K in films thicker than 21 monolayers (ML) in the strong-coupling regime. At the interface, the $LaSi_2$ films bear the tensile strain, leading to the formation of thickness-dependent stripes. The local superconducting gap varies in real space in accordance with the stripes. In some areas with the thickness of 10–21 ML the superconductivity is enhanced, while in films thinner than 10 ML the superconductivity is suppressed due to the suppression of electronic states at the Fermi level. Our work provides insights into the interfacial effects on the superconductivity of epitaxial compound films from both lattice and electronic aspects.

DOI: 10.1103/PhysRevB.100.165308

I. INTRODUCTION

As a benefit from the advance of the precise control of film growth, rich quantum phenomena emerged in the low-dimensional superconducting structures, for example, the superconductor-insulator transition at the two-dimensional (2D) limit [1], and the quantum size effect of the superconductivity in 2D Pb films [2–5]. When the superconductors are in their film forms, the superconducting transition temperature (T_c) can be decreased, e.g., in NbN films on MgO(001) [6], unchanged, e.g., in Al films on Si(111) [7], or increased, e.g., in $La_{1.85}Sr_{0.15}CuO_4$ films on $LaSrAlO_4$ [8], related to the specific substrates and the interfacial atomistic structures [9,10]. The superconducting T_c of single-layer FeSe films on $SrTiO_3$ can even be enhanced by nearly an order of magnitude [11,12]. It is believed that the interfacial effects, both at the electronic and lattice aspects, play the key role in the significant enhancement of superconductivity, while the microscopic mechanism is yet to be clarified [13]. By tuning the thickness with single-layer precision, the BCS superconducting films on Si(111) substrates have been intensively investigated as the prototype [14–18], while it is important to extend the study to complex or unconventional superconducting films.

Lanthanum (La), the first element in lanthanide series, has the electron configuration of $5d^16s^2$ and can be applied to Si-based devices due to the low Schottky barrier height [19,20]. It was reported that polycrystalline films of lanthanum silicide ($LaSi_{2-\alpha}$, $0 \leqslant \alpha \leqslant 0.25$) can be formed by annealing a mass of La on Si surfaces [21]. The recent first-principle calculations pointed out that the single-crystalline $LaSi_2$, with the tetragonal $ThSi_2$ structure of the $I4_1/amd$ space group [22] and the lattice constants of $a_0 = b_0 = 4.28$ Å and $c_0 = 13.72$ Å [Fig. 1(a)], possesses band crossings at the high-symmetry points, suggesting $LaSi_2$ as a potential topologically nontrivial material [23]. In addition, both bulk and thick film of $LaSi_2$ are superconducting with the T_c of 2.3 K (defined as the temperature of the vanishing of DC electrical resistance) [21,24]. The specific heat measurements showed an anomalously small jump at T_c as compared with BCS theory, implying the anisotropy of the Fermi surface or the presence of multiple bands [25]. An in-depth understanding of the superconductivity mechanism is still missing.

In this paper, high-quality $LaSi_2$ films with different thickness (t) are grown by molecular-beam epitaxy (MBE). Since the films bear in-plane tensile strain at the interface, distinct stripes are visible on the thin films by scanning tunneling microscope (STM). The interspacing of the stripes increases with increasing t, indicating the strain relief. By adjusting the film thickness, we focus on the variation of superconducting gap (Δ) and quasiperiodicity of the stripe modulation (d) to investigate the interfacial effects on the superconductivity of $LaSi_2$ films on Si(111) substrate. Electric transport measurements of the films thicker than 72 monolayers (ML, 1 ML = 2.77 Å) show the T_c of 3.2 K. The BCS ratio of the measured superconducting gap to T_c manifests the strong coupling in $LaSi_2$ superconductor. On the surface of the 7–21-ML films, there is the spatial inhomogeneity of the superconducting gap in accordance with the stripes, and in some areas the superconducting gap is enhanced. Further reducing the thickness, the superconductivity is suppressed due to the suppression of the density of states at the Fermi level (E_F) of $LaSi_2$. The thickness-dependent study of the superconductivity of $LaSi_2$

*weihuawang@iphy.ac.cn
†jdguo@iphy.ac.cn

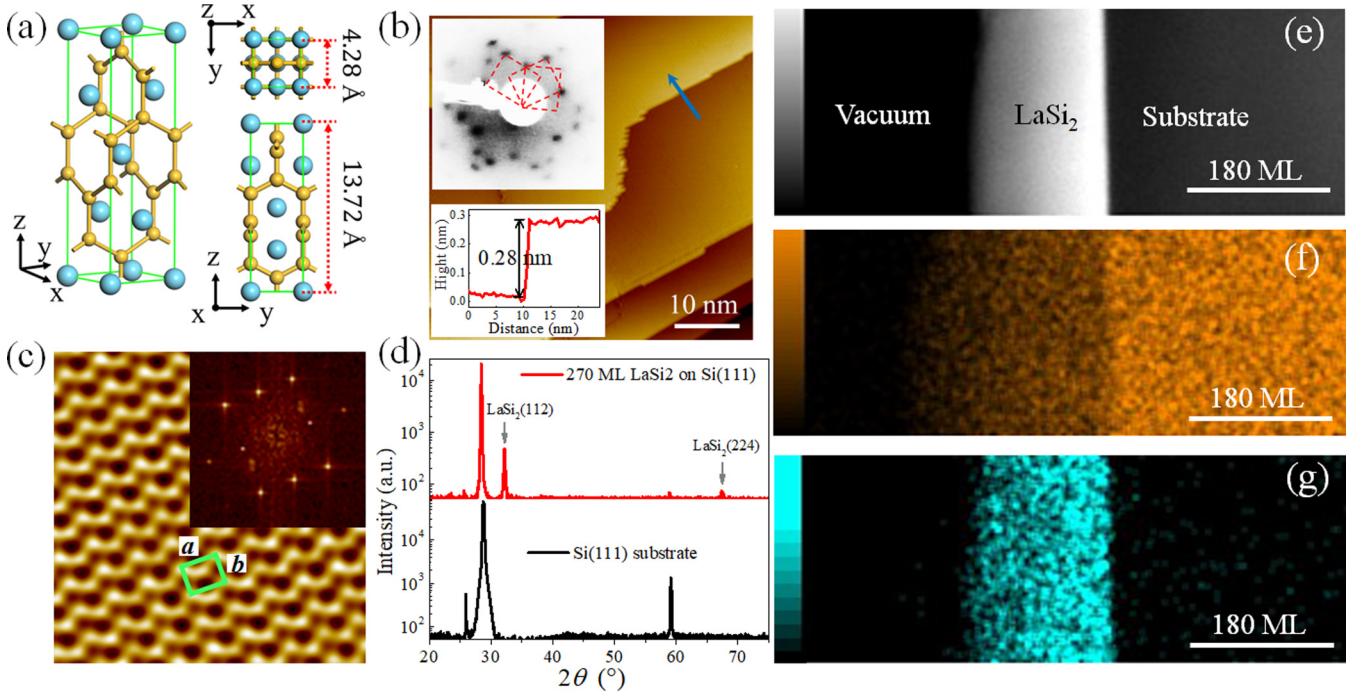

FIG. 1. Structure and morphology of $LaSi_2$. (a) Lattice schematics of $LaSi_2$ in three-dimensional, top, and side views. The blue and yellow spheres represent La and Si atoms, respectively. (b) STM topographic image (−2.4 V/50 pA) of the $LaSi_2$(112) film with the thickness of 108 ML. The upper inset shows the LEED patterns of the $LaSi_2$(112) film, while the lower inset is the height profile of the step marked by the blue arrow. (c) High-resolution STM image (0.5 V/500 pA) of the $LaSi_2$(112) surface, with the in-plane rectangle unit cell labeled. The inset shows the fast Fourier transform of the image. (d) XRD spectra of the 270-ML-thick $LaSi_2$(112) film on Si(111) and the bare Si(111) substrate. The peak at ∼26° is the accompanying diffraction of the Cu K_β line. The results of STEM-EDS of the $LaSi_2$ film with the thickness of 165 ML on Si(111): (e) high-angle annular dark-field image of the $LaSi_2$ film on Si(111); (f), (g) EDS mappings of Si and La, respectively.

films reveals the effects of lattice and electronic modulations as well as their cooperation at the interface.

II. EXPERIMENTAL

The STM experiments were performed in a Unisoku ultrahigh vacuum STM-MBE combined system with the base pressure better than 1×10^{-10} mbar. Commercial Si wafers (0.5 mm thick, *n* type with the room temperature resistance of 0.04 0.08 Ω cm or *p* type with the resistance of 0.02 ∼ 0.04 Ω cm) were cut into 3 × 10-mm^2 pieces as the substrates. The substrate doping type or doping concentration does not influence the results in this paper. The (7 × 7)-reconstructed Si(111) surface was prepared following the standard flashing recipe. High-purity La (Alfa Aesar, 99.9%) was evaporated from a high-temperature effusion cell at 1550 °C to the Si(111) substrates kept at 650 °C. The film thickness was estimated by the La deposition amount and calibrated by STM imaging: for the films thinner than 5 ML, the thickness was determined by directly measuring the height of individual $LaSi_2$ islands, since they coexist with the bare $(\sqrt{3} \times \sqrt{3})$-reconstructed surface. The deposition rate could be therefore determined and the average thickness of thick films be estimated. The *in situ* superconducting gap measurements were performed by scanning tunneling spectroscopy (STS) in differential conductance (dI/dV) spectra at 2.3 K unless otherwise specified. The low-energy electron-diffraction (LEED) measurements were conducted in a separate system with the films prepared under exactly the same conditions as in the STM system. The structures of the $LaSi_2$ films were characterized by *ex situ* x-ray diffractions (XRD) and scanning transmission electron microscopy (STEM). For the STEM measurement, the films were covered by amorphous Si to avoid possible surface deterioration. The *ex situ* four-probe electrical transport measurements were carried out in a commercial physical property measurement system. We only conducted electrical transport measurement for the thick films (>36 ML), where the "buried" $LaSi_2$ layers were protected by the surface layers.

The Vienna *ab initio* Simulation Package was used for density functional theory (DFT) calculations [26,27]. The electron-ion interactions were described by the projector augmented wave [28,29], while the exchange and correlation terms were accounted by the local density approximation [30]. The energy cutoff of 650 eV was used for the expansion of the plane-wave functions. The convergence criteria of the total energy and ionic force loops were set as 10^{-5} eV and 10^{-2} eV $Å^{-1}$, respectively. For Brillouin-zone integration, a *k*-point mesh of 7 × 7 × 1 was set by the Monkhorst-Pack method with the origin at the Γ point. The slabs were built with a vacuum layer of more than 12 Å. To investigate the effects of reduced dimensionality and strain on the electron density of states (DOS), different models were calculated with the parameters as listed in Table I. The lattice constants in model A were fixed as in the bulk $LaSi_2$, while in model B they were relaxed in the calculation. Model C was applied

TABLE I. Parameters of the structural models in DFT calculations.

Model	Lattice constants (Å)	Strain	Relaxation	With substrate
A	$a = 7.52,\ b = 6.05$	No	Disabled	No
B	$a = 7.52,\ b = 6.05$	No	Enabled	No
C	$a = 7.68,\ b = 6.05$	2%	Enabled	No
D	$a = 7.68,\ b = 6.65$	2% + 10%	Disabled	No
E	$a = 7.68,\ b = 6.65$	2% + 10%	Enabled	No
F, G, H	$a = 7.68,\ b = 6.65$	2% + 10%	Enabled	Yes

with 2% tensile strain by enlarging the lattice constant a to 7.68 Å. Model D was applied with 2 and 10% tensile strain along the ***a*** and ***b*** directions, respectively. Model E was relaxed from D. To evaluate the substrate effect on the DOS, the slab models with six Si bilayers covered by 1-, 2-, and 3-ML $LaSi_2(112)$ (marked by F, G, and H) were built. The lattice constants of $LaSi_2$ layer were taken as in model D for simplification. The dangling bonds of the bottom Si layer were saturated by H atoms. The DOS contributed by the top single-layer $LaSi_2(112)$ was extracted.

III. RESULTS AND DISCUSSION

By keeping the Si(111) substrate at a high temperature (∼650 °C) and gradually increasing the La coverage, the surface experiences various one-dimensional reconstructions

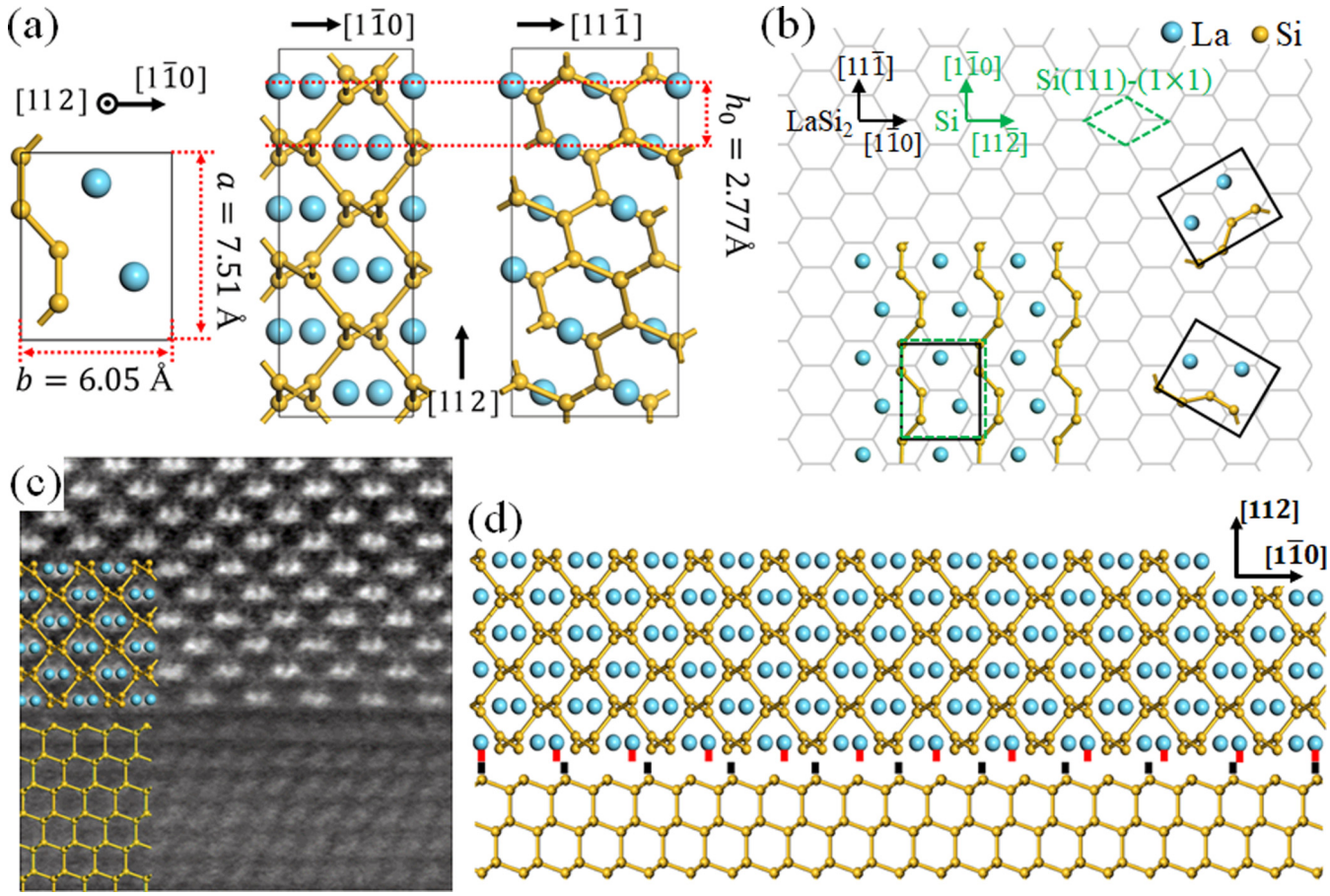

FIG. 2. Crystalline structure of $LaSi_2(112)$ epitaxy on Si(111). (a) Lattice schematics of $LaSi_2(112)$ in top and side views. The crystalline orientation indexes are labeled relative to the $LaSi_2$ lattice. (b) Schematic of the in-plane epitaxial relationship of $LaSi_2(112)$ on Si(111). Three equivalent domains (with the unit cells labeled by the black rectangles) may be formed associated with the threefold symmetry of Si(111). The honeycomb lattice is the Si(111) bilayer with the unit cell labeled by the dashed green rhombus. The green dashed rectangle illustrates the growth template supplied by Si(111) lattice ($2a_0$ and $\sqrt{3}a_0$ along $[1\bar{1}0]$ and $[11\bar{2}]$ directions, respectively, $a_0 = 3.86$ Å) for a "fully strained" epitaxial film. The black rectangle labels the unit cell of $LaSi_2(112)$. The orientation indexes of Si are also labeled in green for reference. (c) STEM image of the $LaSi_2(112)$/Si(111) along $[1\bar{1}0]$ of $LaSi_2$. The lattice schematics of $LaSi_2$ and Si are superimposed. (d) Schematic drawing of the lattice relaxation of $LaSi_2(112)$/Si(111) interface along $[1\bar{1}0]$ of $LaSi_2$. The red and black dots illustrate the lattice alignment.

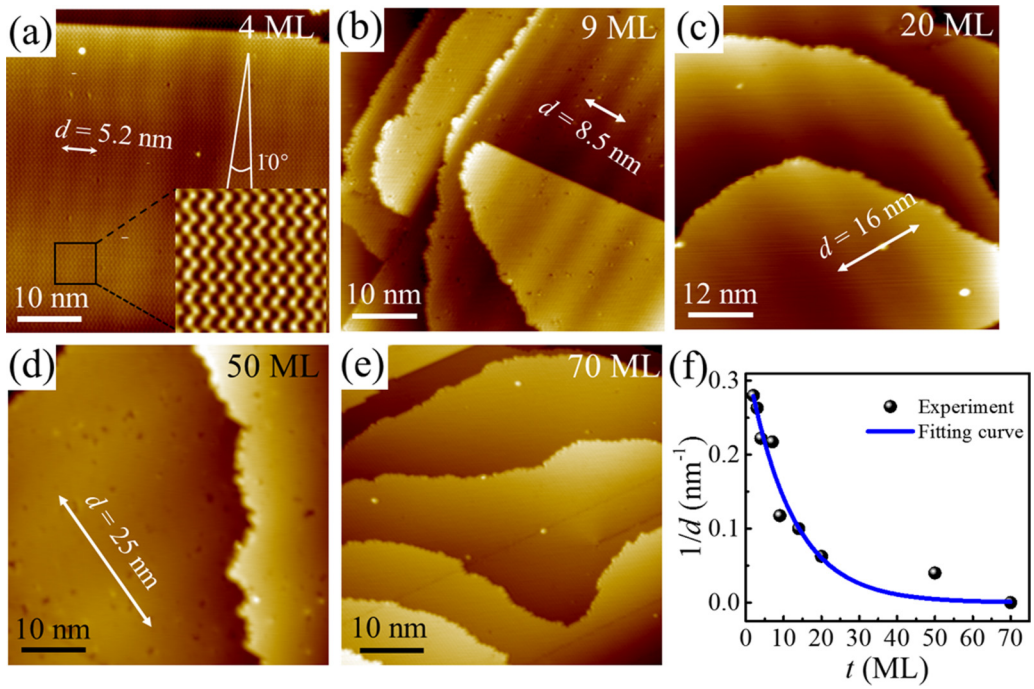

FIG. 3. Stripes on the $LaSi_2(112)$ films with different thickness. (a)–(e) The STM images (−1 V/50 pA) of the $LaSi_2$ surfaces with different thickness. The inset of (a) shows the zoomed-in image. The orientation of the stripes is about 10° off the ***a*** direction of $LaSi_2$ lattice. With the film thickness increasing from 4 to 70 ML, the interspacing of the stripes d increases from 5.2 to >70 nm. (f) The inverse of the stripe interspacing $(1/d)$ as a function of t, fitted by an exponential function $(1/d = 0.33e^{-t/11.77})$.

in the submonolayer region [31]. Further increasing the La dosage, a long-range ordered film is formed. The films appear as separate patches at the initial growth stage, coexisting with the $(\sqrt{3} \times \sqrt{3})$ reconstruction, and form terraced morphologies with increased La coverage. The lattice periodicities of the films are distinct from the underlying Si(111) substrate as well as the single crystal of metal La. On the 108-ML-thick film shown in Fig. 1(b), the terrace height is about 2.8 Å, different from that of Si(111) (3.1 Å). The high-resolution STM image shown in Fig. 1(c) indicates the in-plane rectangular lattice of the film with the unit cell defined by $a = 7.5$ Å and $b = 6.1$ Å. Such periodicity is also visible in the fast Fourier transform of the STM image. The LEED patterns [the upper inset of Fig. 1(b)] show the rectangular periodicity and the existence of three domains in accordance with the equivalent crystalline orientations on Si(111). The XRD results shown in Fig. 1(d) reveal that the epitaxial film is $LaSi_2$ grown in its [112] orientation.

For the growth of the $LaSi_2$ film, the Si substrate serves as the Si source: at the high temperature (650 °C) during the La deposition, sufficient Si atoms were released from the substrate and react with La atoms. We have adjusted the deposition rate of La to allow a sufficient reaction between La and Si. The STEM and energy-dispersive x-ray spectroscopy (EDS) results shown in Figs. 1(e)–1(g) indicate the uniform composition of the films. These characterizations evidence the formation of the stable, uniform, and stoichiometric $LaSi_2$ phase [22]. Although the nonstoichiometry was reported to influence the superconductivity of $LaSi_{2-\alpha}$ films [21,24], it may not play a dominant role in the current work.

The real-space STM images and the reciprocal-space XRD characterizations are consistent with the bulk $LaSi_2(112)$ structure [Fig. 2(a)]: the interlayer spacing of 2.77 Å (along [112] of $LaSi_2$) with the in-plane lattice periodicities of 7.51 Å (along ***a***, $[11\bar{1}]$ of $LaSi_2$) and 6.05 Å (along ***b***, $[1\bar{1}0]$ of $LaSi_2$). Further considering the in-plane epitaxial orientation of the $LaSi_2$ film on Si(111) [Fig. 2(b)], the $LaSi_2$ $[11\bar{1}]$ (***a***) direction is parallel to Si $[1\bar{1}0]$, and $LaSi_2$ $[1\bar{1}0]$ (***b***) is parallel to Si $[11\bar{2}]$. There is a significant lattice mismatch at the interface: 2% along ***a*** and 10% along ***b***. The epitaxial $LaSi_2$ film is subject to a tensile strain along both in-plane directions.

To investigate the microscopic picture of the interfacial lattice relaxation, we carried out the cross-sectional STEM analyses along the $[1\bar{1}0]$ direction of a thick $LaSi_2$ film (165 ML). As shown in Fig. 2(c), the interface is sharp, without any wetting or amorphous layer formed between the $LaSi_2$ film and the Si substrate. Along the $[1\bar{1}0]$ direction of $LaSi_2$, every 11 $LaSi_2$ unit cells are fitted into 10 Si unit cells, as illustrated in Fig. 2(d). The $LaSi_2$ film is almost fully relaxed along ***b***. On the other hand, the $LaSi_2$ film is fully strained along its $[11\bar{1}]$ direction (not shown here), i.e., it bears 2% in-plane tensile strain at the interface along ***a***.

The interfacial lattice relaxation can also be observed in the STM images taken on the films with different thickness. On the 4-ML film, quasiperiodical stripes are observed with the interspacing d of ∼5.2 nm and an angle of 10° off the ***a*** orientation [Fig. 3(a)]. The stripes are irrelevant to the STM scanning conditions, indicating that they reveal the geometric information of the lattice distortion related to the strain relaxation. With the film thickness (t) increasing, the interspacing of the stripes increases gradually [Figs. 3(a)–3(e)] to more

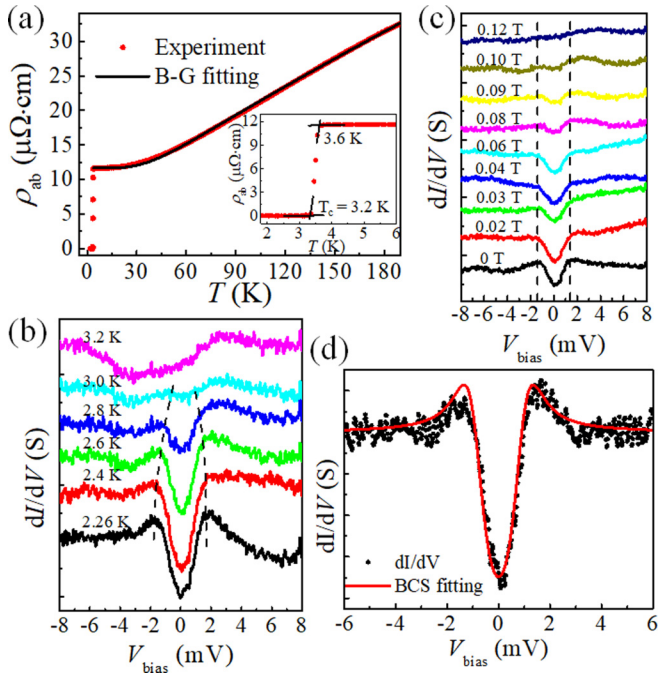

FIG. 4. Superconductivity of $LaSi_2$(112) films measured by electrical transport and STS. (a) ρ_{ab}-T of the 90-ML $LaSi_2$(112) film. The inset shows the zoomed-in curve around T_c. (b), (c) The temperature-dependent dI/dV spectra taken in zero magnetic field and the magnetic-field-dependent dI/dV spectra taken at 2.3 K on the 126-ML $LaSi_2$(112) film, respectively. The spectra are shifted vertically for clear presentation. The black dashed lines indicate the position of the coherent peaks. (d) BCS fitting (red solid curve) of measured superconducting gap (black dots) at 2.3 K of the 126-ML film.

than 70 nm on the 70-ML film (no stripe can be observed in the image of 70 nm × 70 nm). We use $1/d$ to quantitatively represent the degree of strain, which decreases exponentially upon t, as shown in Fig. 3(f). Note that such slight distortion of the $LaSi_2$ lattice associated with the stripes cannot be resolved in TEM.

The four-point electric transport measurements reveal the superconducting behaviors of the thick $LaSi_2$(112) films. As plotted in Fig. 4(a), the temperature-dependent in-plane resistivity ($\rho_{ab} - T$) of the 90-ML film exhibits an abrupt drop at the onset temperature of 3.6 K, and goes to zero at a temperature (defined as the superconducting T_c in this paper) of 3.2 K. In the normal state between 4 and 184 K, the film exhibits metallic behavior. According to Mathiessen's rule, the resistivity can be considered as $\rho_{ab} = \rho_0 + \rho_{ep}(T)$, where ρ_0 is the residual resistivity that reflects the impurity contribution, and $\rho_{ep}(T)$ is governed by the electron-phonon interaction [32] that can be estimated by the Bloch-Grüneisen (B-G) formula [21,33]:

$$\rho_{ep} = \rho' T \left(\frac{T}{\Theta_D}\right)^4 \int_0^{\Theta_D/T} \frac{x^5 dx}{(e^x - 1)(1 - e^x)}, \qquad (1)$$

where ρ' is a constant, and Θ_D the Debye temperature. Fitting the experimental data by the B-G function, we get $\rho_0 = 11.65\ \Omega\,\text{cm}$, $\rho' = 0.48\,\mu\Omega\ \text{cm/K}$, and $\Theta_D = 230$ K. The value of ρ' is consistent with that reported by Travlos and Salamouras [21], while ρ_0 and Θ_D are lower than the reported values [21], evidencing the high quality of the $LaSi_2$ films in the current work.

Figure 4(b) shows the temperature-dependent dI/dV spectra taken *in situ* on the 126-ML $LaSi_2$ film. There is an obvious superconducting gap Δ with pronounced coherence peaks at 2.3 K. With the temperature increasing, the gap is gradually filled up and becomes invisible at 3.2 K. The gap-opening temperature (3.2 K) is consistent with the macroscopic $\rho_{ab} - T$ measurements (in the following, we take the gap-opening temperature as the superconducting T_c for simplicity). The increasing magnetic field also suppresses the superconductivity: the gap gradually closes when the vertical magnetic field reaches 0.1 T at 2.3 K, as shown in Fig. 4(c).

The dI/dV spectra acquired at 2.3 K can be described as the tunneling conductance between a superconductor and a normal metal [34–36]:

$$I(V) = \frac{1}{2\pi} \int_{-\infty}^{\infty} d\varepsilon [f(\varepsilon) - f(\varepsilon + eV)] \times \text{Re}\left(\frac{\varepsilon + eV + i\Gamma}{\sqrt{(\varepsilon + eV + i\Gamma)^2 - \Delta^2}}\right), \qquad (2)$$

where $f(\varepsilon)$ is the Fermi function involving the thermal broadening, Γ the inelastic scattering rate for quasiparticles, and Δ the superconducting gap. We take a gradient of I in Eq. (2) with respect to V, and get the simulated tunneling conductance dI/dV. Then, by optimizing the values of Δ and Γ, the experimental dI/dV spectrum can be fitted. As shown in Fig. 4(d), the fitted value of Δ is 0.9 meV ($\Gamma = 0.2$), giving the superconducting coupling coefficient within the BCS picture as $2\Delta/k_B T_c = 6.52$ (k_B is the Boltzmann constant). It is indicated that the superconductivity of $LaSi_2$ is in the strong-coupling regime.

The dI/dV spectra are measured on the films with different thickness. The values of the Δ, T_c, and $1/d$ (representing the degree of lattice strain) are summarized in Fig. 5(a). While the superconducting characteristics of $LaSi_2$ are unchanged in relatively thick films (above 21 ML), distinct thickness dependence is observed in films thinner than 21 ML. With the thickness decreasing, the superconducting gap increases from 0.9 meV, reaching the maximum of 1.25 meV at 10 ML, and is suppressed significantly at 7 ML [see Fig. 5(b)]. Note that there is significant inhomogeneity of the superconductivity in the films thinner than 10 ML. As shown in Figs. 5(c) and 5(d), the STS spectra exhibit distinct spatial variance in accordance with the stripes on the 7-ML film. The superconducting gaps appear on one side of stripes [the black and green arrows/curves in Figs. 5(c) and 5(d)], while they are significantly suppressed (or even disappear) at other positions. Moreover, we find the superconductivity suppression occurs at different positions relative to the stripes on the film with different thickness (not shown here), since the actual degree of lattice distortion would be different. Here we focus on the maximum values of Δ ($\Delta_{\max}$) measured on each sample with the possible spatial inhomogeneity neglected.

The temperature-dependent dI/dV spectra of the 10-ML film indicate the enhanced T_c (gap-opening temperature) of ~3.5 K, consistent with the enlarged gap. As shown in

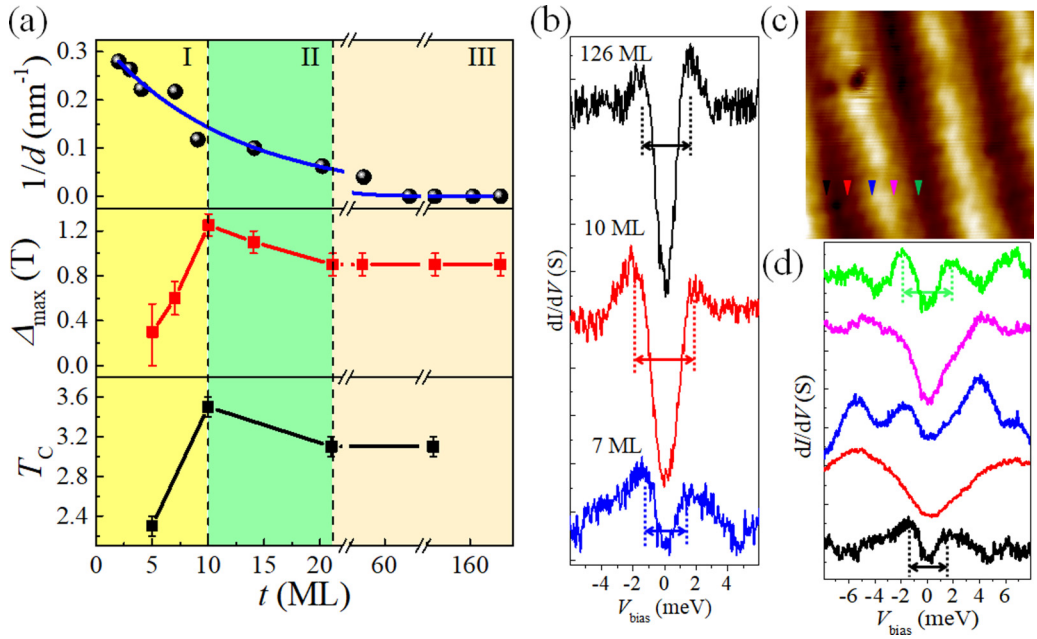

FIG. 5. Interfacial effects on the superconductivity of $LaSi_2$(112) films on Si(111). (a) Thickness-dependent $1/d$ (the blue line is guide to the eye), superconducting gap (the maximum values of Δ_{max} are taken with the spatial inhomogeneity neglected; see the main text), and T_c (taken as the gap-opening temperature). (b) Experimental dI/dV spectra of the films with different thickness measured at 2.3 K. (c) STM image of the stripes on the 7-ML $LaSi_2$ surface. (d) The dI/dV spectra at 2.3 K taken at the positions marked by the arrows in the corresponding colors in (c). All the spectra are normalized following the method described in Ref. [37]. The superconducting gaps are labeled by the dashed lines and arrows, respectively. Note that all the spectra in (b) and (d) are shifted vertically for clear presentation.

Fig. 5(a), the strain, T_c, and Δ_{max} do not change prominently above 21 ML; while they clearly show the consistent increases in the thickness range of $10 \sim 21$ ML. It is evidenced that the superconductivity enhancement is related to the strain at the interface. However, when the thickness is further reduced below 10 ML, Δ_{max} decreases sharply (so as T_c), deviating from the thickness dependence of $1/d$. On the 7-ML film, the superconducting gap is completely closed in some area at 2.3 K [Figs. 5(c) and 5(d)]. One possible reason is that, although the interfacial strain is spatially modulated, in general, it increases with decreasing thickness and could become too large to bestow the superconductivity on the thin $LaSi_2$ films. Additionally, the electronic structures of the thin $LaSi_2$ films change distinctly as observed in the large-scale STS dI/dV spectra. Figure 6(a) shows the suppression of the electron DOS at the Fermi energy (E_F) on the films below 5 ML, and the suppression becomes more prominent with thickness decreasing, accompanied by the disappearance of superconductivity.

To explore the origin of the DOS suppression, we performed the first-principle calculations. For the $LaSi_2$ layers without Si substrate (models A–E as illustrated in Table I), there is no DOS suppression at E_F, even in the freestanding 1-ML $LaSi_2$, regardless of the strain effect (not shown here). The suppression is not purely an effect of reduced dimensionality. Instead, only when the substrate is considered (model F as illustrated in Table I), the calculated partial DOS of the fully strained 1-ML $LaSi_2$ on Si can reproduce the DOS suppression at E_F [Fig. 6(a)]. With the increase of the $LaSi_2$ thickness (models G and H), DOS suppression at E_F gets less prominent. With the spatial distribution of charges at the interface calculated, Fig. 6(b) illustrates the associated microscopic mechanism: The charge density is significantly changed at the epitaxial interface on the $LaSi_2$ side, owing

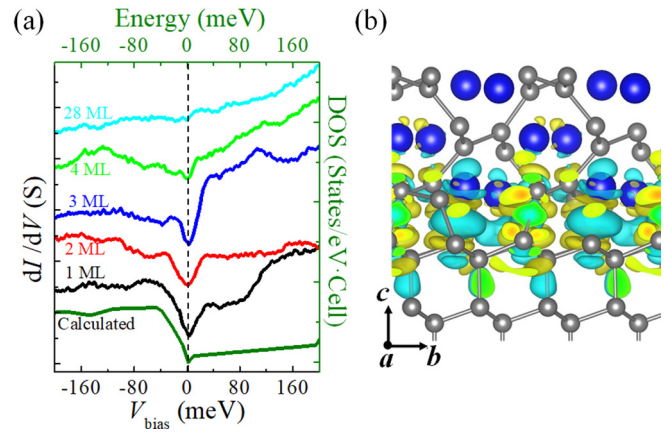

FIG. 6. (a) dI/dV spectra taken at 4.3 K on the $LaSi_2$(112) films with different thickness. The spectra are shifted vertically for clear presentation. The olive curve at the bottom is the calculated DOS of the 1-ML $LaSi_2$(112) on Si(111) for comparison. The reduced DOS of unoccupied states might be related to the interfacial charge redistribution, since such DOS reduction is absent in multilayered $LaSi_2$ (not shown). The vertical dashed line indicates the DOS suppression at E_F in the thin films and the calculated model. (b) Calculated charge redistribution at the $LaSi_2$/Si(111) interface. Cyan (yellow) color represents charge depletion (accumulation) region relative to the pristine $LaSi_2$ and Si, respectively. Blue and gray circles are La and Si atoms, respectively.

to the formation of the chemical bonds between the film and substrate. The superconductivity of the $LaSi_2$/Si(111) is also affected by the interface from the electronic aspect.

In general, the effective range of strain is much longer than the electronic modulations. Since both of them modulate the superconductivity of the $LaSi_2$ films at the interface, the superconducting behaviors can be described in three regimes, characterized by the interfacial effects of strain, electronic modulations, and their cooperation. As shown in Fig. 5(a), in region I where the thickness is below 10 ML, the interfacial effect is dominated by the suppression of DOS at E_F that suppresses the superconductivity. The strain also plays a role, manifested by the inhomogeneous superconductivity associated with the stripes on the surface. Region II (10–21 ML) is dominated by the strain effect. Although the inhomogeneous distribution of lattice distortion results in the slight variation of the local superconducting gap, the Δ value increases with decreasing thickness, suggesting that there is a strain window that enhances the interfacial superconductivity. Region III (above 21 ML) is not significantly affected by the interface, representing the intrinsic superconductivity properties of $LaSi_2$.

IV. CONCLUSIONS

In conclusion, high-quality $LaSi_2$(112) films have been synthesized on Si(111) substrate. The $LaSi_2$ films bear a 2% tensile strain along its [11$\bar{1}$] direction. Consequently, stripes are formed on the film surface, with their interspacing varied with the thickness, representing the degree of the strain relaxation. The thick $LaSi_2$ films (>21 ML) are in the strong-coupling superconducting regime with the superconducting gap of 0.9 meV at 2.3 K and the T_c of 3.2 K. With the film thickness decreasing, the superconductivity is enhanced as the superconducting gap reaching 1.25 meV on the 10-ML film. Besides, the local superconducting gap slightly varies in accordance with the stripes, evidencing the modulation by the interfacial strain. Further decreasing the thickness to less than 10 ML, the superconducting gap decreases sharply. The first-principle calculations reveal the DOS suppression at E_F at the interface. The interfacial effects of strain and electronic modulations with different effective range, as well as their cooperation, lead to the complex variations of the superconducting behaviors, making the $LaSi_2$/Si system an ideal platform to learn the mechanism of interfacial tunings of superconductivity.

ACKNOWLEDGMENTS

The work was supported by the National Key R&D Program of China (Grants No. 2016YFA0202300, No. 2016YFA0300600, and No. 2017YFA0303600), the National Natural Science Foundation of China (Grant No. 11634016), the Strategic Priority Research Program (B) of the Chinese Academy of Sciences (Grant No. XDB07030100), and the Research Program of Beijing Academy of Quantum Information Sciences (Grant No. Y18G09). X.Z. was partially supported by the Youth Innovation Promotion Association of Chinese Academy of Sciences (Grant No. 2016008). W.W. was partially supported by the Hundred Talents Program of the Chinese Academy of Sciences.

L.L. and G.M. contributed equally to this work.

[1] A. M. Goldman and N. Markovic, Phys. Today **51**(11), 39 (1998).
[2] J.-F. Jia, S.-C. Li, Y.-F. Zhang, and Q.-K. Xue, J. Phys. Soc. Jpn. **76**, 082001 (2007).
[3] C. Brun, I-Po Hong, F. Patthey, I. Yu. Sklyadneva, R. Heid, P. M. Echenique, K. P. Bohnen, E. V. Chulkov, and W.-D. Schneider, Phys. Rev. Lett. **102**, 207002 (2009).
[4] Y. Kozuka, M. Kim, C. Bell, B. G. Kim, Y. Hikita, and H. Y. Hwang, Nature (London) **462**, 487 (2009).
[5] S. Qin, J. Kim, Q. Niu, and C.-K. Shih, Science **324**, 1314 (2009).
[6] L. Kang, B. B. Jin, X. Y. Liu, X. Q. Jia, J. Chen, Z. M. Ji, W. W. Xu, P. H. Wu, S. B. Mi, A. Pimenov, Y. J. Wu, and B. G. Wang, J. Appl. Phys. **109**, 033908 (2011).
[7] M. Strongin, O. F. Kammerer, H. H. Farrell, and D. L. Miller, Phys. Rev. Lett. **30**, 129 (1973).
[8] H. Sato and M. Naito, Physica C: Superconductivity **274**, 221 (1997).
[9] D. Valentinis, D. van der Marel, and C. Berthod, Phys. Rev. B **94**, 054516 (2016).
[10] B. Christophe, C. Tristan, and R. Dimitri, Supercond. Sci. Technol. **30**, 013003 (2017).
[11] Q.-Y. Wang, Z. Li, W.-H. Zhang, Z.-C. Zhang, J.-S. Zhang, W. Li, H. Ding, Y.-B. Ou, P. Deng, K. Chang, J. Wen, C.-L. Song, K. He, J.-F. Jia, S.-H. Ji, Y.-Y. Wang, L.-L. Wang, X. Chen, X.-C. Ma, and Q. K. Xue, Chin. Phys. Lett. **29**, 037402 (2012).
[12] D. Huang and J. E. Hoffman, Ann. Rev. Condens. Matter Phys. **8**, 311 (2017).
[13] S. Zhang, T. Wei, J. Guan, Q. Zhu, W. Qin, W. Wang, J. Zhang, E. W. Plummer, X. Zhu, Z. Zhang, and J. Guo, Phys. Rev. Lett. **122**, 066802 (2019).
[14] L. Wang, X. Ma, and Q.-K. Xue, Supercond. Sci. Technol. **29**, 123001 (2016).
[15] E. Rotenberg, H. Koh, K. Rossnagel, H. W. Yeom, J. Schäfer, B. Krenzer, M. P. Rocha, and S. D. Kevan, Phys. Rev. Lett. **91**, 246404 (2003).
[16] T. Zhang, P. Cheng, W. J. Li, Y. J. Sun, G. Wang, X. G. Zhu, K. He, L. L. Wang, X. C. Ma, X. Chen, Y. Y. Wang, Y. Liu, H. Q. Lin, J. F. Jia, and Q. K. Xue, Nat. Phys. **6**, 104 (2010).
[17] M. M. Özer, Y. Jia, Z. Zhang, J. R. Thompson, and H. H. Weitering, Science **316**, 1594 (2007).
[18] M. M. Özer, J. R. Thompson, and H. H. Weitering, Phys. Rev. B **74**, 235427 (2006).
[19] S. Vandré, T. Kalka, C. Preinesberger, and M. Dähne-Prietsch, Phys. Rev. Lett. **82**, 1927 (1999).
[20] H. Yu, L. Wang, M. Schaekers, J. Everaert, Y. Jiang, D. Mocuta, N. Horiguchi, N. Collaert, and K. D. Meyer, IEEE Electron Device Lett. **38**, 843 (2017).
[21] A. Travlos and N. Salamouras, Vacuum **48**, 13 (1997).

[22] M. V. Bulanova, P. N. Zheltov, K. A. Meleshevich, P. A. Saltykov, G. Effenberg, and J. C. Tedenac, J. Alloys Compd. **329**, 214 (2001).
[23] T. Zhang, Y. Jiang, Z. Song, H. Huang, Y. He, Z. Fang, H. Weng, and C. Fang, Nature (London) **566**, 475 (2019).
[24] T. Satoh and Y. Asada, J. Phys. Soc. Jpn. **28**, 263 (1970).
[25] T. Satoh and T. Ohtsuka, Phys. Lett. **20**, 565 (1966).
[26] G. Kresse and J. Hafner, Phys. Rev. B **47**, 558 (1993).
[27] G. Kresse and J. Furthmüller, Phys. Rev. B **54**, 11169 (1996).
[28] G. Kresse and D. Joubert, Phys. Rev. B **59**, 1758 (1999).
[29] P. E. Blöchl, Phys. Rev. B **50**, 17953 (1994).
[30] V. I. Anisimov, I. V. Solovyev, M. A. Korotin, M. T. Czyżyk, and G. A. Sawatzky, Phys. Rev. B **48**, 16929 (1993).
[31] L. Liu, Z. Lin, Y. Wang, W. Wang, F. Yang, X. Zhu, and J. Guo, Surf. Sci. **674**, 40 (2018).
[32] S. I. Vedeneev, A. G. M. Jansen, A. A. Tsvetkov, and P. Wyder, Phys. Rev. B **51**, 16380 (1995).
[33] P. B. Allen and W. H. Butler, Phys. Today **31** (12), 44 (1978).
[34] H. Suderow, P. Martinez-Samper, N. Luchier, J. P. Brison, S. Vieira, and P. C. Canfield, Phys. Rev. B **64**, 020503(R) (2001).
[35] L. Shan, Y.-L. Wang, B. Shen, B. Zeng, Y. Huang, A. Li, D. Wang, H. Yang, C. Ren, Q.-H. Wang, S. H. Pan, and H.-H. Wen, Nat. Phys. **7**, 325 (2011).
[36] R. C. Dynes, J. P. Garno, G. B. Hertel, and T. P. Orlando, Phys. Rev. Lett. **53**, 2437 (1984).
[37] C. Tang, C. Liu, G. Zhou, F. Li, H. Ding, Z. Li, D. Zhang, Z. Li, C. Song, S. Ji, K. He, L. Wang, X. Ma, and Q.-K. Xue, Phys. Rev. B **93**, 020507(R) (2016).